

# Copy Motion From One to Another: Fake Motion Video Generation

Zhenguang Liu<sup>1,2</sup>, Sifan Wu<sup>2\*</sup>, Chejian Xu<sup>1\*</sup>, Xiang Wang<sup>3</sup>, Lei Zhu<sup>4</sup>, Shuang Wu<sup>5</sup> and Fuli Feng<sup>6</sup>

<sup>1</sup>Zhejiang University

<sup>2</sup>Zhejiang Gongshang University

<sup>3</sup>National University of Singapore

<sup>4</sup>Shandong Normal University

<sup>5</sup>Nanyang Technological University

<sup>6</sup>University of Science and Technology of China

{liuzhenguang2008,wusifan2021}@gmail.com, xuchejian@zju.edu.cn, xiangwang@u.nus.edu, leizhu0608@gmail.com, wushuang@outlook.sg, fulifeng93@gmail.com

## Abstract

One compelling application of artificial intelligence is to generate a video of a target person performing arbitrary desired motion (from a source person). While the state-of-the-art methods are able to synthesize a video demonstrating similar broad stroke motion details, they are generally lacking in texture details. A pertinent manifestation appears as distorted *face*, *feet*, and *hands*, and such flaws are very sensitively perceived by human observers. Furthermore, current methods typically employ GANs with a L2 loss to assess the authenticity of the generated videos, inherently requiring a large amount of training samples to learn the texture details for adequate video generation. In this work, we tackle these challenges from three aspects: 1) We disentangle each video frame into foreground (the person) and background, focusing on generating the foreground to reduce the underlying dimension of the network output. 2) We propose a theoretically motivated Gromov-Wasserstein loss that facilitates learning the mapping from a pose to a foreground image. 3) To enhance texture details, we encode facial features with geometric guidance and employ local GANs to refine the face, feet, and hands. Extensive experiments show that our method is able to generate realistic target person videos, faithfully copying complex motions from a source person.

## 1 Introduction

The recent advancement in artificial intelligence has taken the world by storm and given rise to a lot of interesting and compelling applications [Liu *et al.*, 2019b; Liu *et al.*, 2021d; Song *et al.*, 2021; Wang *et al.*, 2021]. Motion copy is one emerging research problem which looks at generating a fake video of a target person performing arbitrary motion, usually

extracted from a source person. While the two person may be vastly different in body shape and appearance, motion copy allows retargeting the motion to the target, empowering an untrained person to be depicted in videos dancing like pop stars [Chan *et al.*, 2019], playing like NBA players, and ma-neuvers in gymnastics and martial arts.

Fundamentally, copying the motion from a source person to a target person amounts to learning a mapping between their video frames. Due to the high dimensionality of this mapping (which renders it almost intractable), it would be more economical to leverage an intermediate representation to bridge the problem. Typically, such approaches include pose-guided and mesh-guided representations, which respectively extract pose or mesh representations from the source person and then learn a generative model that maps this intermediate representation (pose or mesh) to the appearance of the target person. We focus on pose-guided target video generation in this paper.

Upon scrutinizing and experimenting with the released implementations of the state-of-the-art methods, we observe that there are **two key issues** to be addressed. (1) Whereas existing methods achieve plausible results on a broad stroke, the issues of distorted *face*, *hands*, and *feet* are quite rampant and such defects are highly noticeable to the human observer. (2) Current approaches tend to heavily rely on GANs with L2 loss to learn generative models for pose-to-appearance generation. When the training samples for the target person are scarce (typically only a single target video is available), it would be inadequate to learn a competent GAN that typically requires a large amount of training samples to discriminate the authenticity of the generated frames satisfactorily.

To tackle the challenges, we propose a novel motion copy framework *FakeMotion*, consisting of three key designs: 1) We first perform a foreground and background separation. Focusing on foreground generation fundamentally reduces the complexity and dimensionality of the problem. 2) We propose a theoretically motivated Gromov-Wasserstein loss to guide pose-to-appearance generation. The Gromov-Wasserstein loss constitutes an optimal transport objective that learns the pose-to-appearance mapping in a pair-wise

\*Corresponding Authors

fashion, and is more data-efficient and well-suited than conventional GANs for learning the generative model. 3) We refine the textural details of the *face, feet, and hands* with multiple dedicated GANs. In particular, our face refinement adopts a self-supervised approach where we employ geometric cues such as facial orientations to serve as guidance for mining real facial appearances of the target person. These are combined with the coarse generated face for refinement, and the encoding of similar oriented real faces results in more delicate and realistic facial textures. Extensive experiments demonstrate that our method outperforms existing methods.

To summarize, the **key contributions** of this work are: (1) We propose a novel architecture for fake motion video generation, which exploits a Gromov-Wasserstein loss to frame pairwise distance constraint in pose-to-appearance generation. We also present a dense skip connection structure in the generator to facilitate filling the gap between pose and appearance. (2) We further introduce a local enhancement module to explicitly handle the *face, feet, and hands*, which are visually prominent body parts and are often affected by artifacts. (3) Extensive experiments on benchmark datasets demonstrate that our approach achieves new state-of-the-art performance. As a side contribution, we crafted a new dataset for evaluating motion copy methods where 50 subjects in the videos perform complex motions.

## 2 Method

**Problem Statement.** Given two videos, one for the target person whose appearance we want to synthesize, and the other for the source person whose motion we seek to copy [Chan *et al.*, 2019], the goal is to synthesize a video of the target person enacting the same motion as the source person.

**Method Overview.** An overview of our method *Fakemotion* is outlined in Fig. 1. Overall, *Fakemotion* consists of three key stages: a) Data Pre-processing, b) Pose-Guided Appearance Generation, and c) Local Parts Enhancement. Specifically, we *first* extract the pose sequence from the video of the source person. *Then*, we feed the poses into a pose-to-appearance network to synthesize the foreground images of the target person. *Further*, we engage in multiple local GANs to polish the local body parts. *Finally*, the polished foreground is fused with the background, which is extracted from the video of the target person, to approach the final result. We would like to highlight that our generators have an edge in adopting dense skip connections and are equipped with a Gromov Wasserstein loss, while our discriminator games in spatial and temporal dual constraints. In what follows, we elaborate on the key components in detail.

### 2.1 Data Pre-processing

Presented with a video  $V_s$  of the source person and a video  $V_t$  of the target person, we perform the following in parallel: (1) extracting the human pose from each frame of  $V_s$ , and (2) disentangling each frame of  $V_t$  into foreground (person)  $F$  and background  $B$ . The motivations are twofold: (1) The extracted poses of source  $V_s$  unambiguously characterize the motion and can be used to guide appearance generation. (2) Generating the entire image conditioned on a pose might be

too ambitious. Synthesizing only the foreground conditioned on a pose input would reduce the complexity and result in better texture details. Technically, we could adopt off-the-shelf pose estimators [Cao *et al.*, 2019; Liu *et al.*, 2021b; Liu *et al.*, 2022] for pose extraction. For foreground and background decoupling, we follow [He *et al.*, 2017].

### 2.2 Pose-to-appearance Generation

Now, our goal is to generate an appealing foreground image in accordance with a given pose. Particularly, we design a pose-to-appearance generation network, consisting of a *generator* that incorporates dense skip connections and a Gromov-Wasserstein loss, as well as a *discriminator* that enforces spatio-temporal dual constraints.

**Generator with Dense Skip Connections.** As illustrated in Fig. 2, we engage a U-shaped architecture for our pose-to-appearance network. In vanilla U-Net, a decoder layer  $D_i$  is connected to a single encoder layer  $E_i$  and is unable to access low-level features from encoders  $\{E_j\}_{j=1}^{i-1}$ . Consequently, different level features are isolated to each other and their connections are ignored. Building upon the U-Net, we propose to add extra skip connections that help a decoder layer to access lower level features. Instead of connecting a decoder  $D_i$  at layer  $i$  with only the encoder  $E_i$  at layer  $i$ , we allow  $D_i$  to access encoder layers  $\{E_j | j < i\}$ . In this way, each decoder could integrate and fuse feature representations from multiple layers.

**Gromov-Wasserstein Loss to Facilitate Pose-to-appearance Generation.** Our generator network is designed to learn a mapping from a pose  $P_t$  to the corresponding foreground image  $F_t$  of the target person. To enhance temporal consistency, instead of a single pose  $P_t$ , we input a pose context window  $\langle P_{t-1}, P_t, P_{t+1} \rangle$  to the generator. Current methods typically approach this pose-to-appearance problem with a conventional GAN, and measure the discrepancy between the generated foreground and ground truth via a pixelwise L2 loss. However, this inherently requires a large number of training samples in order to generate viable and realistic images. Furthermore, training such GAN models is often precarious and tends to be unstable when adapted to a wide range of target videos. To alleviate this issue, inspired by optimal transport, we propose to measure the generated and ground truth distance via a Gromov-Wasserstein loss, which essentially defines a pairwise distance at the feature-level.

Interestingly, our experiments reveal that our pairwise loss plays an unexpectedly significant role in the model performance. Heuristically, our proposed Gromov-Wasserstein loss looks at the overall distance structure perception. We first extract the VGG features for the generated foreground  $\bar{F}$  and ground truth  $F$ :

$$z^x = \Psi(\bar{F}), z^y = \Psi(F), \quad (1)$$

where  $\Psi(\cdot)$  represents a pre-trained VGG network. The Gromov-Wasserstein loss defines a distance between the metrics on the two feature spaces. We consider two batches of

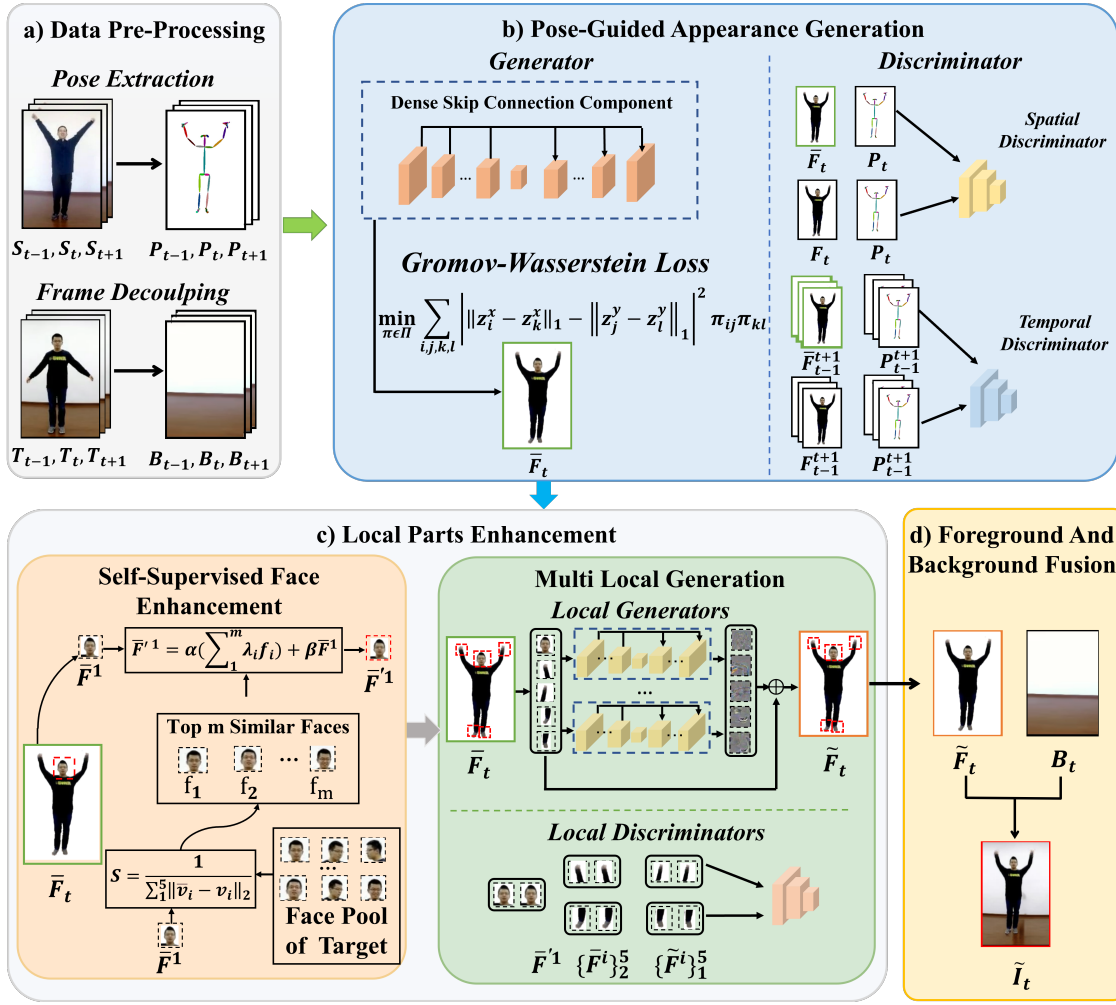


Figure 1: **Overall pipeline.** a) For *data pre-processing*, we extract poses  $\{P_i\}_{i=t-1}^{t+1}$  from source video frames  $\{S_i\}_{i=t-1}^{t+1}$  and decouple the target video frames  $\{T_i\}_{i=t-1}^{t+1}$  into background and foreground. b) The *pose-guided appearance generation* module synthesizes the corresponding foreground image of pose  $P_t$  given a conditioned input of  $\{P_i\}_{i=t-1}^{t+1}$ . We employ a Gromov-Wasserstein loss to facilitate matching of the generated image features with the real image features. Our discriminator assesses spatial-temporal consistency in the video. c) The *local parts enhancement* module refines the details for the *faces, hands and feet*. d) Finally, we *fuse* foreground with the background to generate the entire frame.

feature vectors  $\{z_i^x\}_{i=1}^n, \{z_i^y\}_{i=1}^n$  as two discrete empirical distributions  $\tau, v$ :

$$\tau = \sum_{i=1}^n \frac{1}{n} \delta_{z_i^x}, v = \sum_{i=1}^n \frac{1}{n} \delta_{z_i^y}, \quad (2)$$

where  $\delta$  denotes the Dirac delta distribution. Formally, the Gromov-Wasserstein loss for our task is defined as

$$GW(\tau, v) = \min_{\pi \in \Pi} \sum_{i,j,k,l} \left| \|z_i^x - z_k^x\|_1 - \|z_j^y - z_l^y\|_1 \right|^2 \pi_{ij} \pi_{kl}, \quad (3)$$

where  $\Pi$  denotes the set of point distributions with marginals  $\tau$  and  $v$ . To obtain the Gromov-Wasserstein distance for these

two point distributions, we solve for the optimal transport matrix  $\pi$  that minimizes the squared distance between the intra-space L1 costs. We follow [Peyré et al., 2016] in introducing an entropic regularization term which guarantees tractability (as well as being amenable to backpropagation) in the optimization. We then adopt the Sinkhorn algorithm and projected gradient descent to optimize the entropy regularized Gromov-Wasserstein objectives.

$$C = \left| \|z_i^x - z_k^x\|_1 - \|z_j^y - z_l^y\|_1 \right|^2, \quad (4)$$

$$K = \exp(-C/\varepsilon), \quad (5)$$

$$a \leftarrow \mathbf{1}_n / K b, b \leftarrow \mathbf{1}_n / K^T a, \quad (6)$$

$$\pi = \text{diag}(a) K \text{diag}(b), \quad (7)$$

where  $C$  denotes the cost matrix for a given batch of the gen-

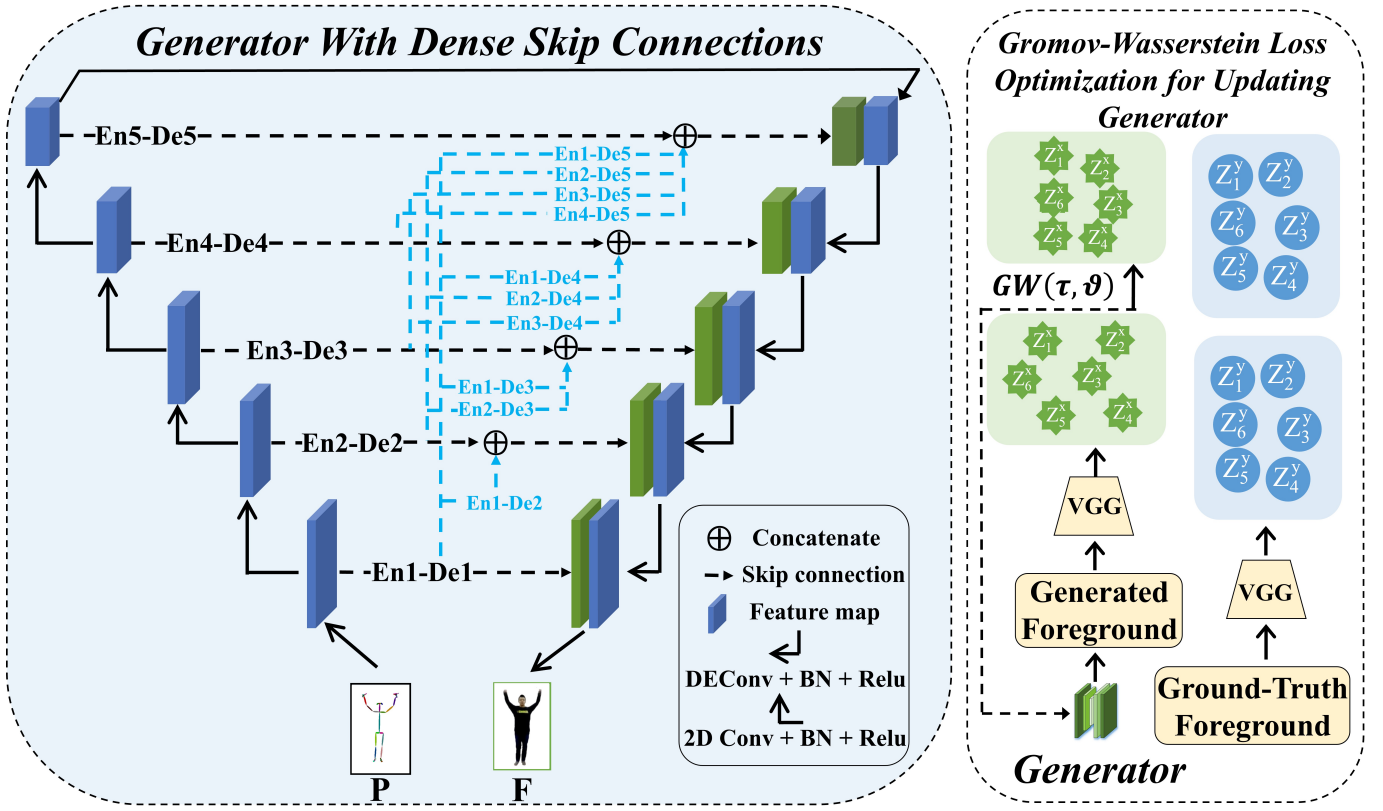


Figure 2: **Generator and Gromov-Wasserstein Loss.** Left: An encoder-decoder architecture with dense skip connections that facilitate the fusion of features across different scales. The blue lines represent the extra connections we added. Right: We introduce the Gromov-Wasserstein loss to update the parameters of the generator and minimize the discrepancy between intra-space distances.

erated foreground features and the ground-truth features.  $\varepsilon$  denotes a regularization coefficient.

Optimizing the Gromov-Wasserstein distance via above equations (Eqs.4–7) updates the generator network parameters through backpropagation. Effectively, this effectuates an alignment of these two feature embedding spaces that facilitates matching of the generated foreground image with the ground-truth. Even when there is scarce training samples for the target person, this pairwise feature matching approach could train the network sufficiently and yield a more detailed and realistic generation. Furthermore, the Gromov-Wasserstein distance is also tractable and stable, and empirically generalizes well to a variety of target video domains.

**Discriminator with Dual Constraints.** Humans generally judge the authenticity of a video from two aspects: the quality of the images and the temporal consistency across frames. The continuity between frames plays a crucial role in visual judgment. Yet, this is often neglected in many existing methods [Dong *et al.*, 2018; Kappel *et al.*, 2021] which tend to focus on single frame quality and cannot explicitly consider temporal continuity. In our approach, we devise dual constraints which are composed of a quality discriminator  $D_q$  and a temporal discriminator  $D_t$ . (1) The quality discriminator  $D_q$  focuses on the single frame quality to assess the authenticity of the forged foreground. (2) The temporal discrim-

inator  $D_t$  is equipped with a set of parallel dilated convolutions that capture temporal information across frames at various temporal scales. As illustrated in Fig. 1,  $D_q$  takes  $(P_t, F_t)$  and  $(P_t, \bar{F}_t)$  as input pairs while the input to  $D_t$  consists of  $(\{P_i\}_{i=t-1}^{t+1}, \{F_i\}_{i=t-1}^{t+1})$  and  $(\{P_i\}_{i=t-1}^{t+1}, \{\bar{F}_i\}_{i=t-1}^{t+1})$ . Both discriminators are trained to classify the authenticity of the generated frame or context window.

### 2.3 Local Parts Enhancement

While the global quality of the generated frames is certainly essential when judging the authenticity of a video, our visual system is also sensitive to prominent body parts, especially the face as well as the hands and feet. When these body parts appear unnatural, our mind would be quick to identify them and judge the videos as fake. Upon experimenting with existing methods following their released codes [Chan *et al.*, 2019; Balakrishnan *et al.*, 2018; Wang *et al.*, 2019; Liu *et al.*, 2019a; Wei *et al.*, 2020], an important insight and conclusion that we draw are that even the state-of-the-art methods still have difficulties in generating natural and realistic details for the face, hands, and feet. Therefore, we introduce a self-supervised face enhancement and additional dedicated local GANs to refine these body parts, with the goal of polishing the texture details on top of the generated results from the pose-to-appearance generation module.

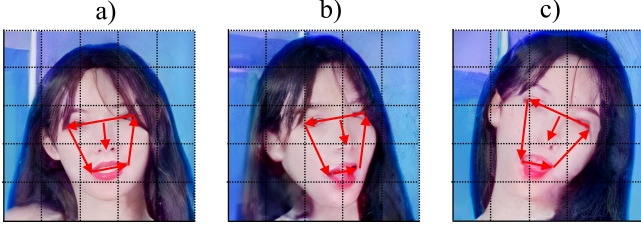


Figure 3: **Face Orientation** is extracted from the face vector field. Three different face orientations are presented.

**Self-Supervised Face Enhancement.** Intuitively, the facial images of the same person should look alike when they are viewed from the similar orientation or viewing angles. With this geometric guidance, we search from the given video of the target person to extract facial images that exhibit similar facial orientations and alignment as that of the synthesized image. This is then leveraged to refine the final face output.

To measure face orientation similarity, we do not simply compute the (cosine) similarity between facial features as the full facial features would usually contain redundant information, *e.g.*, *color and eye shape*, that are irrelevant to face orientation. Instead, we represent facial orientation with vector fields. Specifically, as shown in Fig. 3, we employ 5 vectors, including  $v_1$ : right eye  $\rightarrow$  left eye,  $v_2$ : left eye  $\rightarrow$  left side of the mouth,  $v_3$ : left side of the mouth  $\rightarrow$  right side of the mouth,  $v_4$ : right side of the mouth  $\rightarrow$  right eye,  $v_5$ : the center of eyes  $\rightarrow$  nose. Given two face orientations  $\{v_i\}_{i=1}^5$  and  $\{\bar{v}_i\}_{i=1}^5$ , their similarity can be conveniently computed as:

$$\mathcal{S} = \frac{1}{\sum_{k=1}^5 \|\bar{v}_i - v_i\|_2}, \quad (8)$$

Subsequently, we select top  $m$  ground-truth face images  $\mathbf{f} = \{f_1, \dots, f_m\}$  with the highest similarities as auxiliary faces. Finally, the initially generated face  $\bar{F}^1$  is enhanced into:

$$\bar{F}^1 = \alpha \left( \sum_{i=1}^m (\lambda_i f_i) \right) + \beta \bar{F}^1, \quad (9)$$

where  $\alpha$ ,  $\lambda_i$ , and  $\beta$  are hyperparameters.

**Multi-Local GANs for body parts.** The face enhancement enforces the generated face to be similar to faces with close orientations. We further polish the face and limbs. Similar to the divide-and-conquer strategy in [Liu *et al.*, 2021c], we model each body part with a dedicated local GAN to perform refinement. Specifically, we crop the five key parts  $\bar{F}^1$  (face) and  $\{\bar{F}^i\}_2^5$  (hands, and feet) of the generated foreground image  $\bar{F}_t$ , where  $i$  denotes the  $i^{th}$  key body part. We further feed them into corresponding GANs, which are trained to output a residual image  $F_r^i$ . The residual image reveals the difference in color and texture details between the generated image of the body part and the ground truth. We add them to the generated images to yield the final foreground:

$$\tilde{F}^1 = \bar{F}^1 + F_r^1, \quad (10)$$

$$\tilde{F}^i = \bar{F}^i + F_r^i. \quad (11)$$

**Foreground and Background Fusion.** Finally we may combine the polished foreground  $\tilde{F}_t$  with the inpainted background  $B_t$ . We employ a linear sum to fuse  $\tilde{F}_t$  and  $B_t$  into the final video frame as:

$$\tilde{I}_t = M \odot \tilde{F}_t + (1 - M) \odot B_t \quad (12)$$

where  $M$  is the mask obtained during the pre-processing phase highlighting the region of the foreground.

In practice, for background  $B_t$ , we filled the removed foreground pixels in  $B_t$  following [Yu *et al.*, 2019].

## 2.4 Loss Functions

Now, we zoom in on the loss functions. The proposed Gromov-Wasserstein loss promotes a better learning of the embedding correspondence between the generated foreground space and the ground-truth space. This facilitates extracting commonalities and shared structural similarities between the two spaces.

We further introduce two standard spatial-temporal adversarial losses for  $D_q$  and  $D_t$ , where  $D_q$  enhances the frame-by-frame spatial constraints and  $D_t$  reinforces temporal constraints for every three consecutive frames:

$$L^{spatial} = \mathbb{E}_{(p,I)} [\log D_q(P_t, F_t)] + \mathbb{E}_p [\log(1 - D_q(P_t, G(P_t)))] \quad (13)$$

$$L^{temporal} = \mathbb{E}_{(p,I)} [\log D_t(P_{t-1}^{t+1}, F_{t-1}^{t+1})] + \mathbb{E}_p [\log(1 - D_t(P_{t-1}^{t+1}, G(P_{t-1}^{t+1})))] \quad (14)$$

The Multi Local GANs polish the details of key body parts and we use critics  $D_j$  to present supervision on local details:

$$L_{lr} = \mathbb{E}_I [\log D_j(F^1)] + \mathbb{E}_I [\log(1 - D_j(\bar{F}^1 + G_j(\bar{F}^1)))] + \sum_{j=2}^5 (\mathbb{E}_I [\log D_j(F^j)] + \mathbb{E}_I [\log(1 - D_j(\bar{F}^j + G_j(\bar{F}^j)))]). \quad (15)$$

## 3 Experiments

### 3.1 Experimental Settings

**Datasets.** Experiments are conducted on two benchmark datasets, iPER [Liu *et al.*, 2019a] and ComplexMotion. The **iPER** dataset contains 30 subjects of different shapes, heights and genders. Each subject wears diverse clothes and performs different motions. The whole dataset contains 241,564 frames from 206 videos. Although there are a large number of videos in the iPER, the motions in the videos are relatively common. In order to further examine the performance of the methods on complex motion scenes, *such as doing sophisticated and rapid motion*, we collected a benchmark video dataset, **ComplexMotion**, consisting of 122 in-the-wild videos for more than 50 human subjects. These videos are acquired from various video repositories including TikTok and Youtube. In particular, humans in the dataset wear different clothes and perform complex and rapid movements such as *street dance*, *sports*, and *kung fu*.

Methods	ComplexMotion						iPER					
	Person Reconstruction			Action Imitation			Person Reconstruction			Action Imitation		
	SSIM↑	PSNR↑	LPIPS↓	FID↓	IS↑	TCM↑	SSIM↑	PSNR↑	LPIPS↓	FID↓	IS↑	TCM↑
EDN	0.823	24.36	0.061	64.12	3.411	0.534	0.852	24.48	0.086	57.52	3.305	0.591
FSV2V	0.748	22.51	0.132	99.11	3.164	0.575	0.824	21.18	0.108	107.29	3.136	0.754
PoseWarp	0.711	21.42	0.149	78.21	3.109	0.334	0.792	22.16	0.119	115.23	3.095	0.601
LWGAN	0.789	24.27	0.081	85.30	3.398	0.683	0.843	22.32	0.091	76.38	3.258	0.729
C2F-FWN	0.878	25.68	0.048	53.19	3.408	0.689	0.847	24.32	0.074	60.12	3.412	0.769
SS-FR	0.868	26.44	0.078	54.28	3.349	0.748	0.844	23.23	0.082	61.45	3.337	0.754
MLG	0.872	26.19	0.053	61.49	3.320	0.721	0.848	24.19	0.078	63.22	3.373	0.732
TD	0.865	26.23	0.061	58.71	3.337	0.714	0.832	23.45	0.072	63.76	3.219	0.718
<b>Ours</b>	<b>0.883</b>	<b>27.15</b>	<b>0.040</b>	<b>48.03</b>	<b>3.543</b>	<b>0.773</b>	<b>0.856</b>	<b>25.86</b>	<b>0.068</b>	<b>56.27</b>	<b>3.461</b>	<b>0.799</b>

Table 1: Quantitative results on iPER and ComplexMotion datasets. We quantitatively assess the performance on two scenarios: Person Reconstruction and Action Imitation. ↑ indicates the higher is better, ↓ indicates the lower is better.

Methods	ComplexMotion						iPER					
	Person Reconstruction			Action Imitation			Person Reconstruction			Action Imitation		
	SSIM↑	PSNR↑	LPIPS↓	FID↓	IS↑	TCM↑	SSIM↑	PSNR↑	LPIPS↓	FID↓	IS↑	TCM↑
<b>Our method, Complete</b>	<b>0.883</b>	<b>27.15</b>	<b>0.040</b>	<b>48.03</b>	<b>3.543</b>	<b>0.773</b>	<b>0.856</b>	<b>25.86</b>	<b>0.068</b>	<b>56.27</b>	<b>3.461</b>	<b>0.799</b>
Ablation Analysis of <b>Gromov-Wasserstein loss</b>												
L2 loss	0.836	25.06	0.059	63.62	3.412	0.822	24.10	0.081	64.35	3.168		
Ablation Analysis of <b>Dense Skip Connection</b>												
r/m dense skip connection	0.868	25.28	0.050	62.39	3.218	0.813	24.21	0.075	62.12	3.271		
Ablation Analysis of <b>Self-Supervised Information</b>												
Image feature	0.703	22.42	0.129	83.44	3.215	0.634	22.14	0.108	99.34	3.019		
2 face vectors	0.728	24.68	0.129	78.20	3.108	0.719	21.34	0.114	89.51	3.167		
3 face vectors	0.758	25.62	0.079	56.80	3.331	807	22.56	0.089	73.33	3.267		
4 face vectors	0.784	26.08	0.088	59.71	3.304	0.753	21.52	0.098	75.28	3.261		
1 candidate face	0.732	24.88	0.139	75.20	3.158	0.689	20.24	0.104	88.51	3.067		
2 candidate faces	0.793	26.22	0.083	60.91	3.371	0.746	22.72	0.088	75.54	3.321		
Ablation Analysis of <b>Multiple Local GANs</b>												
r/m multi-local GAN	0.872	26.19	0.053	61.49	3.320	0.848	24.19	0.078	63.22	3.373		

Table 2: Ablation study of different components in our method performed on iPER and ComplexMotion datasets. “r/m X” refers to removing X module in our network. The complete network consistently achieves the best results which are highlighted.

**Implementation details.** During training, all the images are resized to  $512 \times 512$ . We utilize OpenPose to detect the 18 human joints in each frame, which form the pose skeleton. We employ the Mask-RCNN to disentangle each video frame into the foreground and background. We train our model with a mini-batch of 10 for 120 epochs on a Nvidia RTX 2080-Ti GPU. The initial learning rate is set to  $1e-4$ . We employ the Adam optimizer with  $\beta_1 = 0.9$  and  $\beta_2 = 0.999$ .

### 3.2 Comparisons to State-of-the-art Human Motion Copy Methods

To evaluate our approach FakeMotion, we compare it with state-of-the-art approaches including Everybody Dance Now (EDN) [Chan *et al.*, 2019], PoseWarp [Balakrishnan *et al.*, 2018], Few-Shot Video2Video (FSV2V) [Wang *et al.*, 2019], Liquid Warping GAN (LWG) [Liu *et al.*, 2019a], C2F-FWN [Wei *et al.*, 2020], SS-FR, MLG, and TD. Specifically, SS-FR, MLG and TD are three variants of FakeMotion, which correspond to removing the *self-supervised face refinement*, *multiple local GANs*, and *temporal discriminator* from our default method, respectively.

**Quantitative Comparisons.** Following the protocol of existing methods [Liu *et al.*, 2019a; Huang *et al.*, 2021], we

quantitatively benchmark our method and current approaches on two scenes: *Person Reconstruction* and *Action Imitation*. For *Person Reconstruction*, we perform self-imitation where a person mimics motions from themselves. We adopt Structural Similarity (SSIM) [Wang *et al.*, 2004], Peak Signal to Noise Ratio (PSNR) [Korhonen and You, 2012], and Learned Perceptual Image Patch Similarity (LPIPS) [Zhang *et al.*, 2018] to evaluate the quality of the generated image. For *Action Imitation*, we perform cross-imitation where a person mimics another person’s movements. We employ the Inception Score (IS) [Salimans *et al.*, 2016] and Frechet Inception Distance score (FID) [Heusel *et al.*, 2017] as evaluation metrics. To measure the quality of the video instead of image, we also adopt a Temporal Consistency Metric (TCM) [Yao *et al.*, 2017] which concerns temporal consistency. The experimental results on ComplexMotion and iPER are reported in Table 1. Our approach consistently outperforms state-of-the-art methods in both *Person Reconstruction* and *Action Imitation*.

**Qualitative Comparisons.** In addition to quantitative comparisons, we also analyze the generated images visually. Fig. 4 illustrates visual results of six different methods. We observe that PoseWarp and FSV2V suffer from distorted human body and absent hands. EDN achieves plausible visual



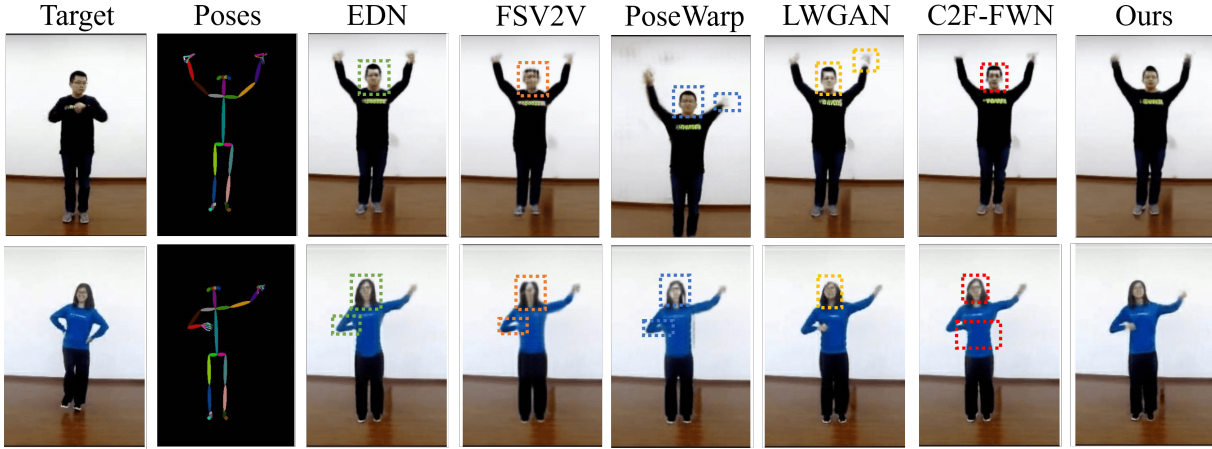


Figure 4: Visualization of the human video motion copy of our method and state-of-the-art approaches. Each column from left to right represents target images, source poses, EDN, FSV2V, PoseWarp, LWGAN, C2F-FWN and our method, respectively. Inaccurate appearances are highlighted with dotted rectangles of different colors. Please zoom in to see more details.

results, however, the face of the person is blurred. Warping-based LWGAN and C2F-FWN are able to effectively copy the motion of source person, but fail to generate fine-grained parts such as hairs and clothing. Our method, in contrast, yields more robust and realistic results on human subjects. We attribute the performance gain to the proposed dense skip connections, Gromov-Wasserstein objective, and the body part GANs.

**Ablation Study.** Extensive ablation experiments are also conducted to investigate the effects of various components. We first investigate the effect of removing *Gromov-Wasserstein loss* in the generator. Specifically, we adopt a traditional L2 loss instead of the Gromov-Wasserstein loss. From Table 2, we observe that SSIM and PSNR fall from 0.883 and 27.15 to 0.836 and 25.06, respectively. These performance deteriorations upon removal of the Gromov-Wasserstein loss suggest the efficacy of the proposed loss. In addition to Gromov-Wasserstein loss, we also investigate the impact of removing *dense skip connections* in the generator. From Table 2, we observe clear performance dips upon removal of the dense skip connection component. This is in line with our intuition that integrating and fusing feature representations from multiple encoder layers are beneficial.

To evaluate the *self-supervised face refinement* module, we consider 1) selecting similar real face images based on facial image features instead of face orientations, 2) using a different number of face vectors, and 3) employing a different number of similar real images. The results of these ablation experiments are reported in Table 2. We observe significant performance drops of SSIM and PSNR upon adopting the first setting. This suggests the effectiveness of using face orientations for similar face searching, which avoids being interfered by unimportant features such as *color* and *eye shape*. Furthermore, we observe that the quality of the generated image gradually increases with the growing of the number of face vectors. Similarly, the increase in the number of used similar real images also leads to better results.

Finally, we also try removing the *multiple local GANs* to evaluate their contributions. Upon the removal, the FID dramatically increases from 48.03 to 61.49 (the smaller the FID value, the better the image quality). This highlights the importance of local refinement. In particular, the residual images, which are produced by the multiple local GANs, disclose the difference in fine-scale texture details between the generated local body parts and the ground-truth, facilitating the generation of more lifelike local images.

## 4 Related Work

**Pose-guided approaches.** The researches learn mapping functions between a pose and its corresponding image [Ren *et al.*, 2020; Zhang *et al.*, 2021; Kappel *et al.*, 2021]. [Ma *et al.*, 2017; Wang *et al.*, 2018] seek high-resolution video2video synthesis by adopting GAN or Two scale-GAN networks. [Yang *et al.*, 2020] performs human video motion transfer in an unsupervised manner, taking advantage of the independence of three orthogonal factors, *motion*, *skeleton*, and *view*. However, these methods fail to take into account the importance of maintaining facial details and the end effectors (*i.e.* hand and feet) in motion transfer. [Chan *et al.*, 2019] introduces a face enhancement module that adopts a traditional GAN architecture.

**Warping-based approaches.** The studies aim to warp the appearance of the target person to copy motions from another person [Balakrishnan *et al.*, 2018; Dong *et al.*, 2018; Liu *et al.*, 2021a; Siarohin *et al.*, 2021]. [Liu *et al.*, 2019a] disentangles the human image into action and appearance, and achieves motion copy using a Warping GAN which warps the image of the target person performing standard actions. [Wei *et al.*, 2020] extracts the motion manifold of the target human and accordingly refines the detailed motion. However, these methods are mesh based, and have inherent difficulties in dealing with irregular shapes and clothing, and also suffer major performance deterioration during rapid motions (unless we have an unlimited number of meshes).

## 5 Conclusion

In this work, we propose a novel fake video generation framework termed *FakeMotion*, which is equipped with dense skip connections, Gromov-Wasserstein GANs, and local enhancement modules. A particular highlight of our method is the Gromov-Wasserstein loss which enables a robust and stable generator training. We further propose a self-supervised face refinement module that resorts to real faces with similar orientations to polish facial details (textures), and multiple local GANs which enhance local details of body parts. Extensive experiments show that our method achieves notable improvements and is able to handle rapid-motion and complex scenes.

## Acknowledgements

This research is supported by the National Key R&D Program of China (Grant no.2018YFB1404102), the National Natural Science Foundation of China (No. 61902348), the Key R&D Program of Zhejiang Province (No. 2021C01104), and the Postgraduate Research Innovation Fund Project of Zhejiang Gongshang University.

## References

- [Balakrishnan *et al.*, 2018] Guha Balakrishnan, Amy Zhao, Adrian V Dalca, Fredo Durand, and John Guttag. Synthesizing images of humans in unseen poses. In *Proceedings of the IEEE Conference on Computer Vision and Pattern Recognition*, pages 8340–8348, 2018.
- [Cao *et al.*, 2019] Zhe Cao, Gines Hidalgo, Tomas Simon, Shih-En Wei, and Yaser Sheikh. Openpose: realtime multi-person 2d pose estimation using part affinity fields. *IEEE transactions on pattern analysis and machine intelligence*, 43(1):172–186, 2019.
- [Chan *et al.*, 2019] Caroline Chan, Shiry Ginosar, Tinghui Zhou, and Alexei A Efros. Everybody dance now. In *Proceedings of the IEEE/CVF International Conference on Computer Vision*, pages 5933–5942, 2019.
- [Dong *et al.*, 2018] Haoye Dong, Xiaodan Liang, Ke Gong, Hanjiang Lai, Jia Zhu, and Jian Yin. Soft-gated warping-gan for pose-guided person image synthesis. *arXiv preprint arXiv:1810.11610*, 2018.
- [He *et al.*, 2017] Kaiming He, Georgia Gkioxari, Piotr Dollár, and Ross Girshick. Mask r-cnn. In *Proceedings of the IEEE international conference on computer vision*, pages 2961–2969, 2017.
- [Heusel *et al.*, 2017] Martin Heusel, Hubert Ramsauer, Thomas Unterthiner, Bernhard Nessler, and Sepp Hochreiter. Gans trained by a two time-scale update rule converge to a local nash equilibrium. *Advances in neural information processing systems*, 30, 2017.
- [Huang *et al.*, 2021] Zhichao Huang, Xintong Han, Jia Xu, and Tong Zhang. Few-shot human motion transfer by personalized geometry and texture modeling. In *Proceedings of the IEEE/CVF Conference on Computer Vision and Pattern Recognition*, pages 2297–2306, 2021.
- [Kappel *et al.*, 2021] Moritz Kappel, Vladislav Golyanik, Mohamed Elgharib, Jann-Ole Henningson, Hans-Peter Seidel, Susana Castillo, Christian Theobalt, and Marcus Magnor. High-fidelity neural human motion transfer from monocular video. In *Proceedings of the IEEE/CVF Conference on Computer Vision and Pattern Recognition*, pages 1541–1550, 2021.
- [Korhonen and You, 2012] Jari Korhonen and Junyong You. Peak signal-to-noise ratio revisited: Is simple beautiful? In *2012 Fourth International Workshop on Quality of Multimedia Experience*, pages 37–38. IEEE, 2012.
- [Liu *et al.*, 2019a] Wen Liu, Zhixin Piao, Jie Min, Wenhan Luo, Lin Ma, and Shenghua Gao. Liquid warping gan: A unified framework for human motion imitation, appearance transfer and novel view synthesis. In *Proceedings of the IEEE/CVF International Conference on Computer Vision*, pages 5904–5913, 2019.
- [Liu *et al.*, 2019b] Zhenguang Liu, Shuang Wu, Shuyuan Jin, Qi Liu, Shijian Lu, Roger Zimmermann, and Li Cheng. Towards natural and accurate future motion prediction of humans and animals. In *Proceedings of the IEEE/CVF Conference on Computer Vision and Pattern Recognition*, pages 10004–10012, 2019.
- [Liu *et al.*, 2021a] Wen Liu, Zhixin Piao, Zhi Tu, Wenhan Luo, Lin Ma, and Shenghua Gao. Liquid warping gan with attention: A unified framework for human image synthesis. *IEEE Transactions on Pattern Analysis and Machine Intelligence*, 2021.
- [Liu *et al.*, 2021b] Zhenguang Liu, Haoming Chen, Runyang Feng, Shuang Wu, Shouling Ji, Bailin Yang, and Xun Wang. Deep dual consecutive network for human pose estimation. In *Proceedings of the IEEE/CVF Conference on Computer Vision and Pattern Recognition*, pages 525–534, 2021.
- [Liu *et al.*, 2021c] Zhenguang Liu, Kedi Lyu, Shuang Wu, Haipeng Chen, Yanbin Hao, and Shouling Ji. Aggregated multi-gans for controlled 3d human motion prediction. In *Proceedings of the AAAI Conference on Artificial Intelligence*, volume 35, pages 2225–2232, 2021.
- [Liu *et al.*, 2021d] Zhenguang Liu, Pengxiang Su, Shuang Wu, Xuanjing Shen, Haipeng Chen, Yanbin Hao, and Meng Wang. Motion prediction using trajectory cues. In *Proceedings of the IEEE/CVF International Conference on Computer Vision*, pages 13299–13308, 2021.
- [Liu *et al.*, 2022] Zhenguang Liu, Runyang Feng, Haoming Chen, Shuang Wu, Yixing Gao, Yunjun Gao, and Xiang Wang. Temporal feature alignment and mutual information maximization for video-based human pose estimation. *arXiv preprint arXiv:2203.15227*, 2022.
- [Ma *et al.*, 2017] Liqian Ma, Xu Jia, Qianru Sun, Bernt Schiele, Tinne Tuytelaars, and Luc Van Gool. Pose guided person image generation. *arXiv preprint arXiv:1705.09368*, 2017.
- [Peyré *et al.*, 2016] Gabriel Peyré, Marco Cuturi, and Justin Solomon. Gromov-wasserstein averaging of kernel and



- distance matrices. In *International Conference on Machine Learning*, pages 2664–2672. PMLR, 2016.
- [Ren *et al.*, 2020] Yurui Ren, Ge Li, Shan Liu, and Thomas H Li. Deep spatial transformation for pose-guided person image generation and animation. *IEEE Transactions on Image Processing*, 29:8622–8635, 2020.
- [Salimans *et al.*, 2016] Tim Salimans, Ian Goodfellow, Wojciech Zaremba, Vicki Cheung, Alec Radford, and Xi Chen. Improved techniques for training gans. *Advances in neural information processing systems*, 29:2234–2242, 2016.
- [Siarohin *et al.*, 2021] Aliaksandr Siarohin, Oliver J Woodford, Jian Ren, Menglei Chai, and Sergey Tulyakov. Motion representations for articulated animation. In *Proceedings of the IEEE/CVF Conference on Computer Vision and Pattern Recognition*, pages 13653–13662, 2021.
- [Song *et al.*, 2021] Xue Song, Jingjing Chen, Zuxuan Wu, and Yu-Gang Jiang. Spatial-temporal graphs for cross-modal text2video retrieval. *IEEE Transactions on Multimedia*, 2021.
- [Wang *et al.*, 2004] Zhou Wang, Alan C Bovik, Hamid R Sheikh, and Eero P Simoncelli. Image quality assessment: from error visibility to structural similarity. *IEEE transactions on image processing*, 13(4):600–612, 2004.
- [Wang *et al.*, 2018] Ting-Chun Wang, Ming-Yu Liu, Jun-Yan Zhu, Guilin Liu, Andrew Tao, Jan Kautz, and Bryan Catanzaro. Video-to-video synthesis. *arXiv preprint arXiv:1808.06601*, 2018.
- [Wang *et al.*, 2019] Ting-Chun Wang, Ming-Yu Liu, Andrew Tao, Guilin Liu, Jan Kautz, and Bryan Catanzaro. Few-shot video-to-video synthesis. *arXiv preprint arXiv:1910.12713*, 2019.
- [Wang *et al.*, 2021] Zheng Wang, Jingjing Chen, and Yu-Gang Jiang. Visual co-occurrence alignment learning for weakly-supervised video moment retrieval. In *Proceedings of the 29th ACM International Conference on Multimedia*, pages 1459–1468, 2021.
- [Wei *et al.*, 2020] Dongxu Wei, Xiaowei Xu, Haibin Shen, and Kejie Huang. C2f-fwn: Coarse-to-fine flow warping network for spatial-temporal consistent motion transfer. *arXiv preprint arXiv:2012.08976*, 2020.
- [Yang *et al.*, 2020] Zhuoqian Yang, Wentao Zhu, Wayne Wu, Chen Qian, Qiang Zhou, Bolei Zhou, and Chen Change Loy. Transmomo: Invariance-driven unsupervised video motion retargeting. In *Proceedings of the IEEE/CVF Conference on Computer Vision and Pattern Recognition*, pages 5306–5315, 2020.
- [Yao *et al.*, 2017] Chun-Han Yao, Chia-Yang Chang, and Shao-Yi Chien. Occlusion-aware video temporal consistency. In *Proceedings of the 25th ACM international conference on Multimedia*, pages 777–785, 2017.
- [Yu *et al.*, 2019] Jiahui Yu, Zhe Lin, Jimei Yang, Xiaohui Shen, Xin Lu, and Thomas S Huang. Free-form image inpainting with gated convolution. In *Proceedings of the IEEE/CVF International Conference on Computer Vision*, pages 4471–4480, 2019.
- [Zhang *et al.*, 2018] Richard Zhang, Phillip Isola, Alexei A Efros, Eli Shechtman, and Oliver Wang. The unreasonable effectiveness of deep features as a perceptual metric. In *Proceedings of the IEEE conference on computer vision and pattern recognition*, pages 586–595, 2018.
- [Zhang *et al.*, 2021] Jinsong Zhang, Kun Li, Yu-Kun Lai, and Jingyu Yang. Pise: Person image synthesis and editing with decoupled gan. In *Proceedings of the IEEE/CVF Conference on Computer Vision and Pattern Recognition*, pages 7982–7990, 2021.